22

Chemical and Biosensing Applications Based on Graphene Field-Effect Transistors

Yasuhide Ohno, Kenzo Maehashi and Kazuhiko Matsumoto
The Institute of Scientific and Industrial Research, Osaka University
Japan

1. Introduction

Label-free electrical detection of biomolecule based on nano-meter size materials has attracted in many fields such as clinical diagnosis for health care, life science and practical pharmacy because they are expected for rapid and easy detection of various biological species at home. Chemical and biological sensors using silicon nanowires(Cui et al., 2001; Li et al., 2005; Zheng et al., 2005) and carbon nanotubes (CNTs)(Besteman et al., 2003; Chen et al., 2003; Ishikawa et al., 2010; Maehashi et al., 2007; Maehashi, Matsumoto, Kerman, Takamura & Tamiya, 2004; Martnez et al., 2009; Star et al., 2003) have been developed for the past decades. Especially, CNT field-effect transistors (CNT-FETs) are one of the strongest candidates for biosensing applications due to their high aspect ratio, high mechanical strength, large surface areas and outstanding electrical characteristics. These superior characteristics make CNTs ideal for nanoscale devices(Saito et al., 1998). There have been many reports about chemical and biological sensors using CNT-FETs such as proteins, glucose, DNA hybridizations and immunosensors(Besteman et al., 2003; Chen et al., 2003; Ishikawa et al., 2010; Maehashi et al., 2007; Maehashi, Matsumoto, Kerman, Takamura & Tamiya, 2004; Martnez et al., 2009; Star et al., 2003).

Although the CNT-FET based sensors have high potential, their electrical characteristics strongly depends on their chirality (diameter) and work function of the contact metal(Chen et al., 2005). Since the chirality control growth of CNTs has not been achieved, the reproducibility and stability of the CNT-FET based sensors have been major problem(Maehashi, Ohno, Inoue & Matsumoto, 2004). And the typical absolute value of the drain current (I_D) of a CNT-FET with one CNT channel in solution is several nA to several 10 nA because only small drain and gate voltages can be applied in solution due to the avoidance of solution electrolysis and oxidization of the electrodes, channel and analyte. To resolve these problems, aligned CNTs have been studied in recent years(Palaniappan et al., 2010). However, the separation between semiconductor and metallic CNTs is also very difficult problem.

Graphene, single layer hexagonal network of carbon atom, can modify these problems. Since they are ideal two-dimensional crystal with extremely high carrier mobility at room temperature without any sophisticated doping process and very stable materials, graphene field-effect transistors (G-FETs) have been expected for the next-generation practical devices(Geim & Novoselov, 2007; Novoselov et al., 2004). In recent years, sensing applications using graphene and graphene-like materials have been intensively studied because their electrical characteristics are very sensitive for the environmental conditions and

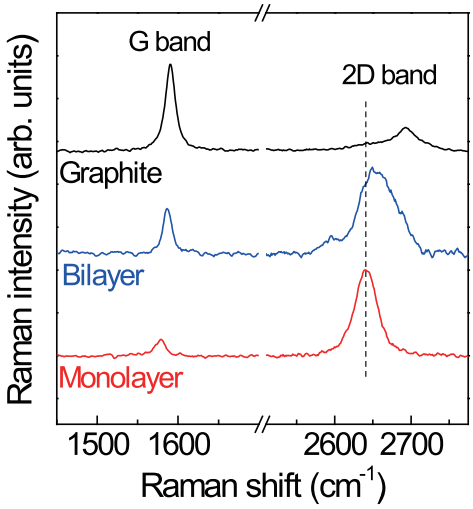

Fig. 1. Raman spectra of G- and 2D-bands for 1 and 2 layer(s) graphene and HOPG.

the surface-analyte or analyte-analyte bindings occur very close to the graphene channel(Yang et al., 2010). The mechanism of action for G-FET sensors is that chemical species adsorbed on the surface of the graphene act as electron donors or acceptors, resulting in conductance changes. Most of the graphene sensors have been used to detect gas molecules(Arsat et al., 2009; Dan et al., 2009; Fowler et al., 2009; Lu et al., 2009; Qazi et al., 2007; Robinson et al., 2008; Schedin et al., 2007). In addition, research on electrical detection of biomolecule detection using graphene has gradually increased over the last few years. Electrochemical detections of glucose and proteins have been investigated(Alwarappan et al., 2009; Lu et al., 2007; Shan et al., 2009; Shang et al., 2008; Wu et al., 2009). Field-effect transistors based on reduced graphene from graphene oxide or graphene amine have detected DNA hybridizations and negatively charged bacteria(Mohanty & Berry, 2008). In graphene, the highest carrier mobility is only achieved in single-layer graphene due to its linear energy dispersion at K point(Nagashio et al., 2008). Since the sensitivity using G-FET-based chemical and biological sensors depend on their transconductance ($= \partial I_D/\partial V_G = C_G V_D \mu$; where C_G, V_D and μ are the gate capacitance, drain voltage and field-effect mobility, respectively), G-FETs with single-layer graphene are thought to be suitable for the sensing devices.

In this chapter, we describe our attempts to apply G-FETs with single-layer graphene to chemical and biological sensors(Ohno et al., 2009). We investigated behavior of G-FETs immersed in an electrolyte and show that they have very good transfer characteristics compared with their characteristics in vacuum. They also exhibit clear pH-dependent I_D characteristics and could electrically detect surface-protein adsorption. Moreover, we demonstrate the achievement of electrical detection of biomolecules and their charge types by G-FETs.

2. Experimental

The G-FETs used in this study were fabricated on a 285-nm-thick thermally grown SiO_2 layer on a heavily *p*-doped silicon substrate ($\rho < 0.01\ \Omega$·cm). Single-layer graphene flakes were obtained by micromechanical exfoliation using natural graphite and clear adhesive tape. The graphene flakes were searched by an optical microscope after slowly peeling off the tape from the substrate. As a result of this procedure, various types of graphene layers (or thick graphite) were identified on the surface SiO_2/Si substrate. Single-layer graphene flakes were identified by analyzing the shift in green intensity under optical microscope observation and by Raman spectroscopy. Figure 1 compares the 632.8 nm Raman spectra of 1 and 2 layer(s) graphene and highly oriented pyrolytic graphite (HOPG). Two strong peaks with a G band at $\sim$1580 cm^{-1} and a 2D band at $\sim$2650 cm^{-1} could be observed. A single peak of the 2D can be observed for the single-layer graphene, while a much broader peak with some shoulders, shifted to a high-frequency, could be observed for the bilayer graphene. As shown in Figure 1, a single peak in the 2D band in the Raman spectrum is direct evidence of single-layer graphene(Ferrari et al., 2006). Ti (5 nm)/Au (30 nm) source and drain electrodes were formed by electron beam lithography and lift-off method. The degenerately doped silicon substrate was also used for the back gate. Typical optical microscope image of G-FET was shown in Fig. 2.

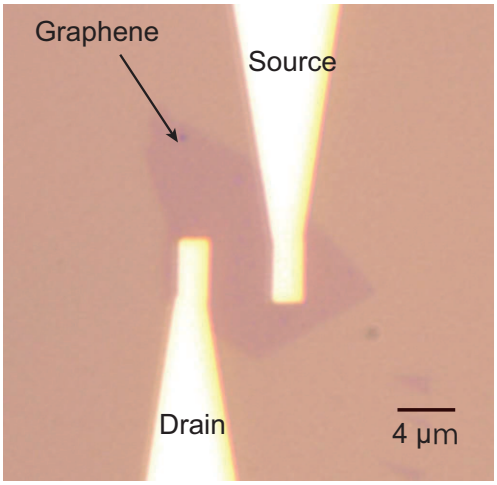

Fig. 2. Optical micrograph of a typical G-FET.

To measure the solution pH value and protein adsorption, the device was surrounded by a silicone rubber pool attached to the substrate. Then, the Ag/AgCl reference electrode was immersed into the solution contained within a silicone rubber barrier as shown in Fig. 3 and Fig. 4. The Ag/AgCl reference electrode was used as the top-gate electrode to minimize environmental effects(Minot et al., 2007). The electrical characteristics of the G-FETs were measured by a semiconductor parameter analyzer (4156C; Agilent technologies Inc., Santa Clara, CA), using two-terminal measurement. In the experiments, we drove the G-FETs under low voltage ($\leq$ 0.2 V) due to the avoidance of oxidization of electrodes and graphene channel. Natural graphite used in this work was kindly provided by Nippon Graphite Industries Ltd. (Shiga, Japan). 10 mM phthalate buffer solution of pH 4.0, phosphate buffer solution of pH 6.8 and 10 mM borate buffer solution at pH 9.3 were purchased from Horiba Ltd. (Kyoto, Japan).

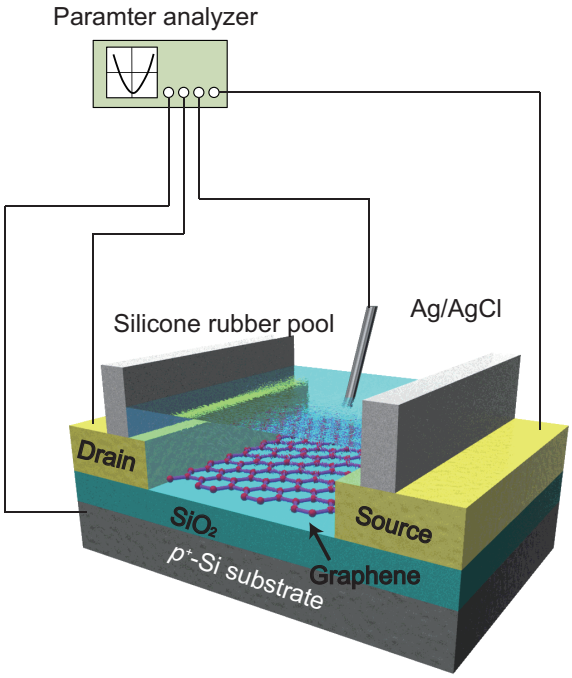

Fig. 3. Schematic illustration of experimental setup with G-FETs.

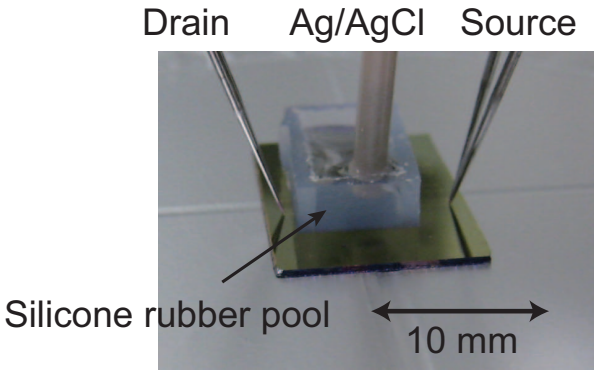

Fig. 4. Photograph of experimental setup with a G-FET.

Solutions of various pH values were prepared by mixing a 10 mM phthalate buffer solution of pH 4.0, a 10 mM phosphate buffer solution of pH 6.8 and a 10 mM borate buffer solution at pH 9.3. Bovine serum albumin (BSA), which was used as the target protein, was purchased from Sigma Aldrich Inc. (St Louis, MO).

3. Results and discussion

3.1 Transport characteristics in solution

At first, we investigated the transport characteristics of G-FETs in solution. In a solution or electrolyte, the electrical-double layer acts as a top-gate insulator, and the thickness of electrical-double layer is generally defined by the Debye-Hückel equation, which depends on the ionic strength and temperature, which is as small as 5 nm in the buffer solution with several ten mM. This value is very thin compared with the SiO_2 layer used as the back-gate insulator. For graphene devices, only 90 or 290 nm-thick SiO_2 can be used because single or a few layer graphene flakes on the 90 or 290 nm can be observed by a conventional optical microscope due to the refractive index of the graphene(Blake et al., 2007). Because of this thin gate insulator, the field-effect applied by the top-gate electrodes is very effective compared from the back gate. In fact, electrolyte-gated CNT-FETs and G-FETs have shown good electrical characteristics as thin top-gate insulators with high dielectric constants in ionic solutions(Das et al., 2008; Rosenblatt et al., 2002).

A typical plot of I_D as a function of back-gate voltage under reduced pressure (1×10^{-3} Pa) is shown in Fig. 5. Transconductance ($= \partial I_D / \partial V_G$) was estimated to be 0.13 μS and 30 μS for back-gate and top-gate operations, respectively. The transconductance was for top-gate operation was more than 200 times better than that of back-gate operation; thus, a thin electrical-double layer is formed on the graphene surface. This result shows that G-FETs can operate even in solution, and their electrical characteristics in solution are excellent.

To clarify the difference between the g_m values of the devices, back- and top-gate capacitances were estimated using a simple model. Assuming that graphene is equivalent to a metal disk placed on the insulator, the gate capacitance can be expressed by the equation below, (Gelmont et al., 1995)

$$C_G = \frac{2\pi\varepsilon_0(\varepsilon_r + 1)r}{\tan^{-1}\left[\frac{2h(\varepsilon_r + 1)}{r\varepsilon_r}\right]}, \tag{1}$$

where, r, h, ε_r and ε_0 are the radius of the metal disk (graphene), the thickness of the gate insulator, the relative permittivity and vacuum permittivity, respectively. For the electrolyte-gated G-FETs (with r=1.5 μm, h=1 nm and ε_r (H_2O)=80), the estimated electrostatic gate capacitance was C_{G_EL} ~500 nF cm^{-2}. In this case, if total top-gate capacitance (C_{TG}) is considered as a series of the C_{G_EL} and the quantum capacitance (C_Q), (Meric et al., 2008; Rosenblatt et al., 2002) then C_{TG}=$C_{G\_EL}C_Q/(C_{G\_EL} + C_Q)$. Because the C_Q of the graphene channel is approximately 2 μF cm^{-2}, (Meric et al., 2008) the C_{TG} is 400 nF cm^{-2}. This value is more than three orders of magnitude larger than the back-gate capacitance of 85 pF cm^{-2} (with r=1.5 μm, h=285 nm and ε_r (SiO_2)=3.9), given by the above equation. It can be concluded that this larger top-gated capacitance gave rise to better transfer characteristics of G-FETs in the electrolyte, indicating their high potentials for use in field-effect sensing applications.

3.2 pH dependence

The dependence of the transfer characteristics and conductance of G-FETs on pH were evaluated. Figure 6 shows I_D plotted as a function of V_{TGS} for a G-FET in various electrolytes at various pH values from 4.04 to 8.16. The Dirac points of the G-FET shifted in a positive detection with increasing pH. This behavior indicates that G-FETs can detect the pH value by the electrical characteristics. A plot of the time-dependent I_D for a G-FET at V_{TGS} =−80 mV in pH values from 4.0 to 8.2. is shown in Figure 7. Every 10 min, either a 10-mM phosphate buffer solution at pH 6.8 or a 10-mM borate buffer solution at pH 9.3 were added to increase

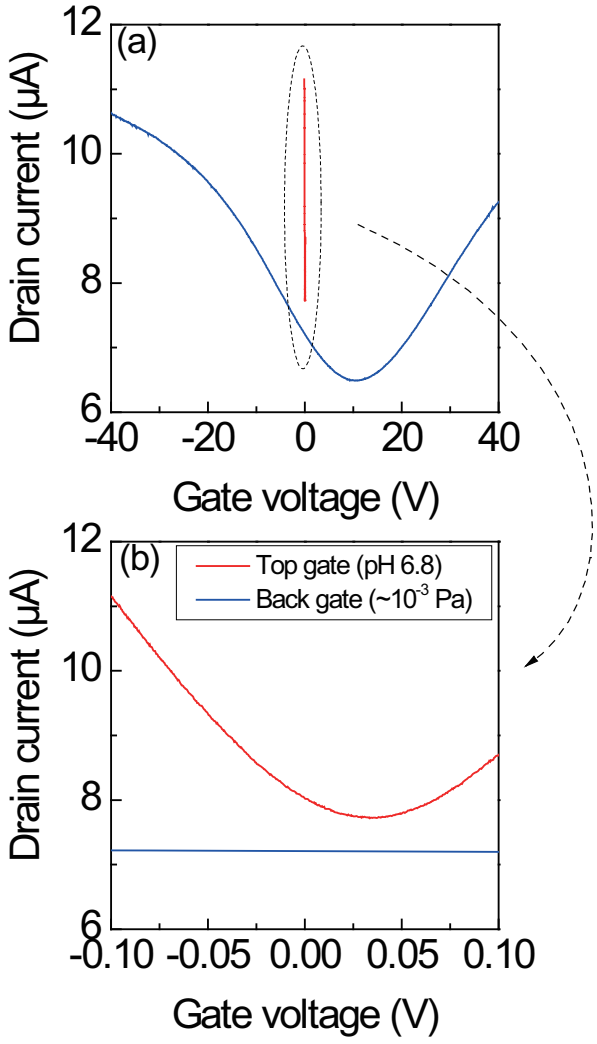

Fig. 5. (a) I_D as a function of back-gate voltage at 10^{-3} Pa and top-gate voltage in an solution at pH 6.8. (b) Enlarged view of I_D as a function of gate voltage.

the pH. The I_D increased stepwise with pH from 4.0 to 8.2, and the I_D at each pH value was virtually constant. The plot of the average I_D against pH values indicates that the relationship between pH and I_D is linear over the range from 4.0 to 8.2, as shown in Figure 8. Similar changes in gate transfer characteristics have been observed for a G-FET exposed to NO_2 and pH dependence of G-FETs with few-layer epitaxial graphene. It is concluded that the increased I_D can be attributed to the increased negative charge around the graphene channel, because the hole is the carrier in this condition. The origin of the increase in current is not clear at present. We speculate that hydrogen or hydroxide ions have some effect on the graphene surface. In case of the CNT-FETs, hydroxide ions bound to the carbon nanotube surface act as acceptors(Lee et al., 2007; Pan et al., 2004). As a nano-carbon material, graphene may exhibit chemical reactivity similar to carbon nanotubes. Further investigation is necessary to clarify this point.

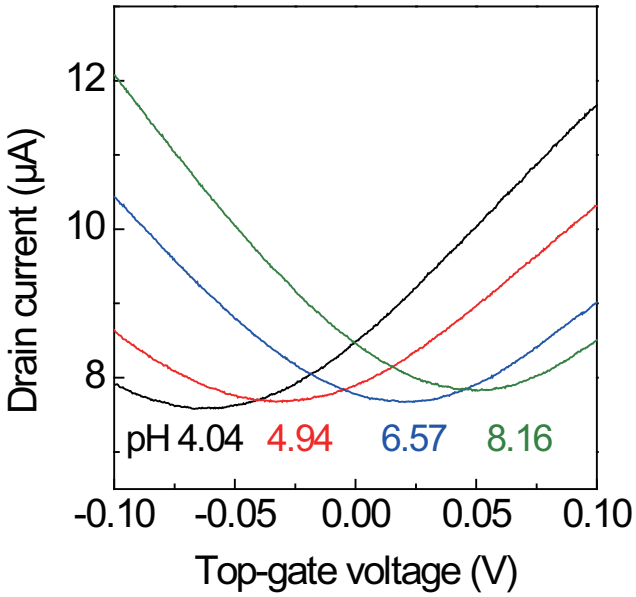

Fig. 6. I_D as a function of top-gate voltage of a G-FET at pH 4.04, 4.94, 6.57 and 8.16.

It should be noted that the Dirac point of G-FETs at a pH solution was not constant. Although the Dirac point = 0 V was realized at pH 5.8 in this device, other devices showed the Dirac point = 0 V at different pH values. One possible reason of the instability is due to charged impurities such as residual EB resist, defects or underlying SiO_2 and Si. Indeed, the solution pH slightly influenced the carrier mobility. Charged impurity scattering is major subject in the graphene technology. These uncontrollable charged impurities may lead the Dirac point instability.

The detection limit (=resolution, signal/noise=3) for changes in pH was estimated to be 0.025 in the pH range from 4.04 to 8.16. In this work, the signal and noise were defined by the average and standard deviation of the data, respectively. On the other hand, a pH sensor based on carbon nanotube FETs showed the detection limit of 0.67 due to the small drain current in

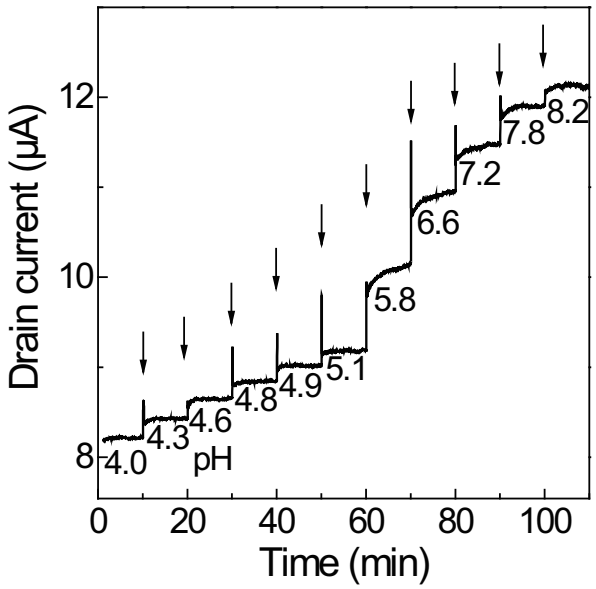

Fig. 7. I_D versus time data of a G-FET for pH values from 4.04 to 8.16. Arrows indicate the adding points of solution with different pH.

solution ($\sim$ 10 nA)(Yamamoto et al., 2009). Therefore, the G-FETs are useful as pH sensors for their stability. The pH dependence of the drain current was similar to that of few-layer epitaxial graphene.

3.3 Detection of protein adsorption

Finally, we demonstrated label-free biomolecule detection, based on electrolyte-gated G-FETs. A 10-mM phosphate buffer electrolyte solution at pH 6.8 was used, with a bovine serum albumin (BSA; Sigma Aldrich Inc., St Louis, MO) target biomolecule. The isoelectric point of BSA is 5.3, indicating that BSA molecules are negatively charged at the pH used for this measurement. Figure 9 shows the evolution of I_D of a G-FET for electronic monitoring of BSA adsorption on a graphene channel at $V_{TGS} = -0.1$ V and $V_{BGS} = 0$ V. Under this condition, the I_D was expected to be increased by the hole carrier when (negatively charged) BSA was attached to the graphene. Measurement began with a 10-mM pure phosphate buffer solution. After 10 min, further pure buffer solution was added and I_D was virtually unchanged. After 20 min, BSA concentration dependence of I_D was shown. Arrows in Figure 9 mark the points where solutions with various concentration of BSA were injected. The I_D clearly increased when BSA was introduced, indicating adsorption on the graphene surface. The drain current change (ΔI_D) is shown as a function of BSA concentration (C_{BSA}) in Figure 10. ΔI_D increased linearly at low concentrations and was saturated at higher concentrations. This result indicates that the adsorption of BSA molecules onto the graphene surface follows the Langmuir adsorption isotherm given by

$$\frac{C_{BSA}}{\Delta I_D} = \frac{C_{BSA}}{\Delta I_{DMax}} + \frac{K_d}{\Delta I_{DMax}}, \tag{2}$$

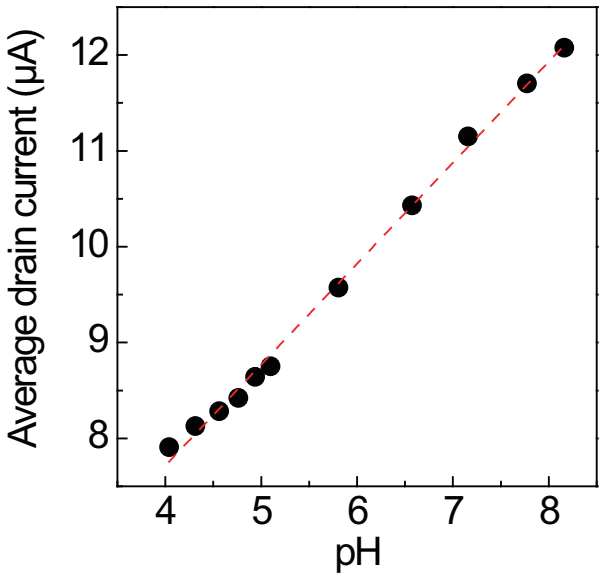

Fig. 8. Average I_D as a function of pH. The dashed line is a linear fit to the data points.

where K_d is the dissociation constant of the interaction between BSA molecules and graphene and ΔI_{DMax} is the drain current at saturation. The Langmuir adsorption isotherm fitted the experimental results well, as shown in Figure 10 (red dashed line). The K_d was estimated to be 1.5×10^{-8} M, which was comparable with the values obtained for Si nanowire(Cui et al., 2001) and CNT-FET biosensors(Abe et al., 2008; Maehashi et al., 2009) using antibody-antigen interactions, despite the fact that BSA molecules were considered to be directly adsorbed onto the graphene surface in this work rather than through a protein-protein interaction. Further experiments are needed to confirm the suitability of the Langmuir adsorption isotherm for these experimental results.

Moreover, adsorption of proteins with different charge types onto the graphene surface was detected. The isoelectric point of BSA is approximately 5.3; accordingly, BSA molecules are positively (negatively) charged in the 10-mM phthalate (phosphate) buffer solution. Four G-FETs were used in this experiment. Two of them were used in the phthalate buffer solution and others in the phosphate buffer solution. Figures 11 show the time course of normalized I_D at V_D and V_{TGS} of 0.1 and -0.1 V, respectively. The drain current decreased when 80 (red lines) and 100 (blue lines) nM BSA in 10 mM phthalate buffer solution (pH 4.0) was added, indicating that the graphene channel detected the positive charge. Conversely the drain current increased after adding negatively charged BSA in 10 mM phosphate buffer solution (pH 6.8). And the I_D changes seem to depend on the concentration of BSA. It should be noted that some I_D trends are unstable after adding the BSA as shown in Fig. 11. The origin of these unstable features may come from remote impurity in SiO_2 layer under the graphene channel. Very recent research showed that the existence of SiO_2 layer influenced the sensing properties for G-FETs.

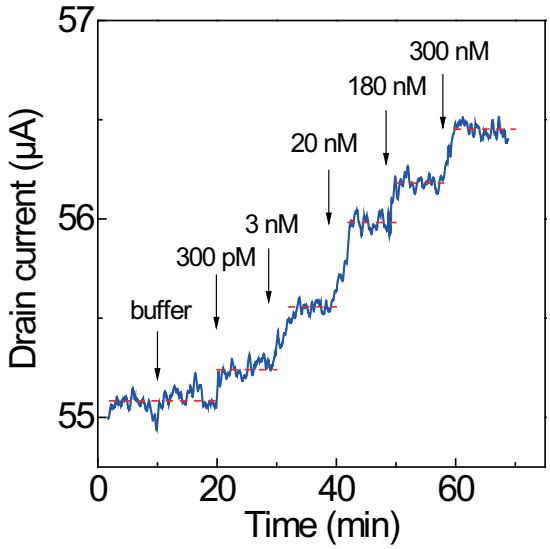

Fig. 9. I_D versus time for electrical monitoring of exposure to various BSA concentrations. Dashed lines indicate the average I_D.

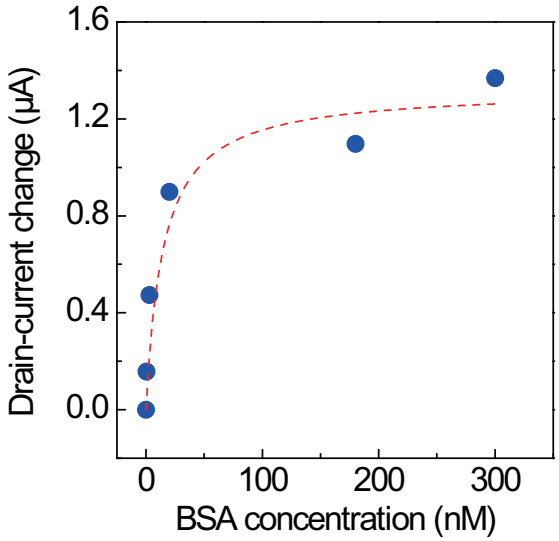

Fig. 10. Plot of the net I_D change of a G-FET versus BSA concentration. The dashed line is a fit to the Langmuir adsorption isotherm.

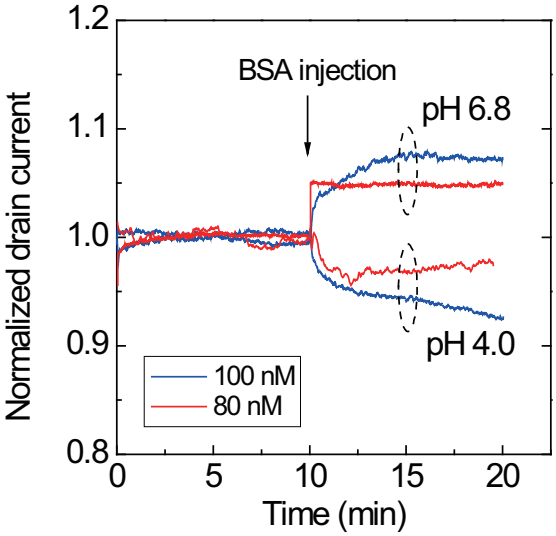

Fig. 11. Time course of normalized I_D for G-FETs at V_D and V_{TGS} of 0.1 and −0.1 V, respectively, in 10-mM phthalate and phosphate buffer solution. Red (blue) lines indicate that 80 (100) nM BSA was added at 10 min.

These results indicate that the graphene channel could detect the charge type of the adsorbed biomolecules. Under the experimental conditions, the carriers in the graphene channel were holes. Therefore, the decreased (increased) I_D observed for BSA in the phthalate (phosphate) buffer solution was a consistent result, because the hole carrier in the graphene channel decreased (increased) as a result of exposure to the positively (negatively) charged proteins. For biosensors based on CNT-FETs, only positive charged biomolecules can be detected, owing to their *p*-type semiconductor band characteristics(Yamamoto et al., 2010). In contrast, the G-FETs can detect positively and negatively charged biomolecules because a Schottky barrier does not form at the interface between the electrodes and graphene, owing to its the zero-gap semiconductor characteristics. Furthermore, the absolute value of the drain current is larger than that of carbon nanotube devices, indicating their robustness to noise.

In this work, the conductance changes by BSA adsorption were quite small. Three possible interpretations can be considered for the small conductance changes. One interpretation is due to the electrode-graphene contact resistance. Although two-terminal measurement was used in this experiment, four-terminal measurement is needed to ignore the contact resistance fluctuations. Another interpretation is due to desorption of the BSA molecules. Protein sensing using specific protein detection such as antigen-antibody effect is efficiency to interrupt the BSA desorption. The other interpretation is due to the difference between isoelectric point of the BSA (=5.6) and solution pH (=6.8) is relatively small. This small difference may lead some uncharged amino acid of the BSA molecules. Moreover, it is important to clarify where the charge transfer occurs and surface area dependence of the protein adsorption. These subjects should be investigated to develop the biomolecule detector using G-FETs.

The G-FETs can reuse after measuring of protein adsorption. Figure 12 shows the optical micrographs of a G-FET after exposing the several μM BSA (a) and after washing the proteins

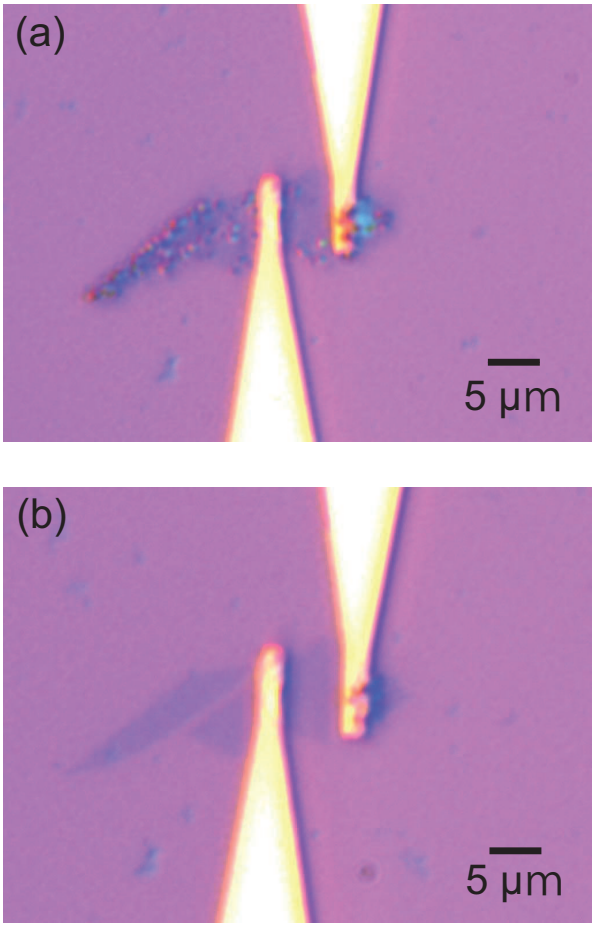

Fig. 12. Optical micrograph of a G-FET (a) after exposing proteins and (b) washing the proteins by acid and alkali solutions.

by acid and alkali solutions (b). Many bright points indicate the adsorbed proteins onto the graphene surface, and only these proteins disappeared after washing by sulfuric acid and sodium hypochlorite solution. The graphene flakes have not been broken by these solutions, indicating their high stability. And after the washing process, the G-FET can reuse as a sensor. These results indicate that the G-FETs have high potentials for the chemical and biological sensors.

3.4 Comparison of the CNT-FETs and G-FETs

Finally, comparison of the sensing characteristics of CNT-FETs and G-FETs are briefly described. The important requirements of materials for the sensing device are the charge sensitivity and stability. Since the charge sensitivity is strongly depends on the surface to volume ratio, it can be considered that the CNT-FETs have better charge sensitivity than G-FETs. On the contrary, the stability of G-FETs is superior to the CNT-FETs. Their absolute

value of the drain current is as high as several ten μA, which is more than 1000 times larger than those of CNT-FETs. This large drain current indicates the robustness for the noise during the sensing measurements. The stable devices carry more credibility. And chirality-controlled CNT growth technique, which leads the stable FET characteristics, has not been achieved at present. This problem makes it difficult to fabricate the integrated sensors based on CNT-FETs. In the case of G-FETs, the development of growth technique of graphene is the key technology. Very recent reports says the roll-to-roll production of 30-inch graphene films can be grown by CVD system(Bae et al., 2010). Such large-scale graphene growth technique will lead large-scale integrated and multiple sensors based on G-FETs. Because both CNT-FETs and G-FETs have superior characteristics for the sensing applications each other, it is important to use them according to the situations.

4. Conclusion

We have investigated chemical and biological sensors using G-FETs. Single-layer graphene was obtained by a micro-mechanical cleavage method. Changes in the solution pH were electrically detected with a lowest detection limit (signal/noise = 3) of the 0.025. Their I_D showed protein-concentration dependence and their I_D changes with BSA concentration were fitted well by the Langmuir adsorption isotherm. In addition, the G-FETs clearly detected the different charge types of a biomolecule owing to its isoelectric point. G-FETs are promising devices for highly sensitive chemical and biological sensors. In near future, we try to evaluate the selective protein sensing using the G-FETs.

5. References

Abe, M., Murata, K., Ataka, T. & Matsumoto, K. (2008). Calibration method for a carbon nanotube field-effect transistor biosensor, *Nanotechnology* 19: 045505.

Alwarappan, S., Erdem, A., Liu, C. & Li, C.-Z. (2009). Probing the Electrochemical Properties of Graphene Nanosheets for Biosensing Applications, *J. Phys. Chem. C* 113: 8853–8857.

Arsat, R., Breedon, M., Shafiei, M., Spizziri, P., Gilje, S., Kaner, R., Kalantar-zadeh, K. & Wlodarski, W. (2009). Graphene-like nano-sheets for surface acoustic wave gas sensor applications, *Chem. Phys. Lett.* 467: 344–347.

Bae, S., Kim, H., Lee, Y., Xu, X., Zheng, J.-S. P. Y., Balakrishnan, J., Lei, T., Kim, H. R., Song, Y. I., Kim, Y.-J., Kim, K. S., Özyilmaz, B., Ahn, J.-H., Hong, B. H. & Iijima, S. (2010). Roll-to-roll production of 30-inch graphene films for transparent electrodes, *Nat. Nanotechnol.* 5: 574–578.

Besteman, K., Lee, J.-O., Wiertz, F. G. M., Heering, H. A. & Dekker, C. (2003). Enzyme-Coated Carbon Nanotubes as Single-Molecule Biosensors, *Nano Lett.* 3: 727–730.

Blake, P., Hill, E. W., Neto, A. H. C., Novoselov, K. S., Jiang, D., Yang, R., Booth, T. J. & Geim, A. K. (2007). Making graphene visible, *Appl. Phys. Lett.* 91: 063124.

Chen, R. J., Bangsaruntip, S., Drouvalakis, K. A., Kam, N. W. S., Shim, M., Li, Y., Kim, W., Utz, P. J. & Dai, H. (2003). Noncovalent functionalization of carbon nanotubes for highly specific electronic biosensors, *Proc. Natl. Acad. Sci.* 100: 4984–4989.

Chen, Z., Appenzeller, J., Knoch, J., lin, Y. & Avouris, P. (2005). The Role of Metal-Nanotube Contact in the Performance of Carbon Nanotube Field-Effect Transistors, *Nano Lett.* 5: 1497–1502.

Cui, Y., Wei, Q., Park, H. & Lieber, C. M. (2001). Nanowire Nanosensors for Highly Sensitive and Selective Detection of Biological and Chemical Species, *Science* 293: 1289–1292.

Dan, Y., Lu, Y., Kybert, N. J., Luo, Z. & Johnson, A. T. C. (2009). Intrinsic Response of Graphene Vapor Sensors, *Nano Lett.* 9: 1472–1475.

Das, A., Pisana, S., Chakraborty, B., Piscanec, S., Saha, S. K., Waghmare, U. V., Novoselov, K. S., Krishnamurthy, H. R., Geim, A. K., Ferrari, A. C. & Sood, A. K. (2008). Monitoring dopants by Raman scattering in an electrochemically top-gated graphene transistor, *Nat. Nanotechnol.* 3: 210–215.

Ferrari, A. C., Meyer, J. C., Scardaci, V., Casiraghi, C., Lazzeri, M., Mauri, F., Piscanec, S., Jiang, D., Novoselov, K. S., Roth, S. & Geim, A. K. (2006). Raman Spectrum of Graphene and Graphene Layers, *Phys. Rev. Lett.* 97: 187401.

Fowler, J. D., Allen, M. J., Tung, V. C., Yang, Y., Kaner, R. B. & Weiller, B. H. (2009). Practical Chemical Sensors from Chemically Derived Graphene, *ACS Nano* 3: 301–306.

Geim, A. K. & Novoselov, K. S. (2007). The rise of graphene, *Nat. Mater.* 6: 183–191.

Gelmont, B., Shur, M. S. & Mattauch, R. J. (1995). Disk and Stripe Capacitances, *Solid-State Elec.* 38: 731–734.

Ishikawa, F. N., Chang, H.-K., Curreli, M., Liao, H.-I., Olson, C. A., Chen, P.-C., Zhang, R., Roberts, R. W., Sun, R., Cote, R. J., Thompson, M. E. & Zhou, C. (2010). Label-Free, Electrical Detection of the sars Virus N-Protein with Nanowire Biosensors Utilizing Antibody Mimics as Capture Probes, *ACS nano* 3: 1219–1224.

Lee, K., Kwon, J. H., Cho, S. M. W. S., Ju, B. K. & Lee, Y. H. (2007). pH sensitive multiwalled carbon nanotubes, *Mat. Lett.* 61: 3201–3203.

Li, C., Curreli, M., Lin, H., Lei, B., Ishikawa, F. N., Datar, R., Cote, R. J., Thompson, M. E. & Zhou, C. (2005). Complementary Detection of Prostate-Specific Antigen Using In_2O_3 Nanowires and Carbon Nanotubes, *J. Am. Chem. Soc.* 127: 12484–12485.

Lu, G., Ocola, L. E. & Chen, J. (2009). Gas detection using low-temperature reduced graphene oxide sheets, *Appl. Phys. Lett.* 94: 083111.

Lu, J., Drzal, L. T., Worden, R. M. & Lee, I. (2007). Simple Fabrication of a Highly Sensitive Glucose Biosensor Using Enzymes Immobilized in Exfoliated Graphite Nanoplatelets Nafion Membrane, *Chem. Mater.* 19: 6240–6246.

Maehashi, K., Katsura, T., Kerman, K., Takamura, Y., Matsumoto, K. & Tamiya, E. (2007). Label-Free Protein Biosensor Based on Aptamer-Modified Carbon Nanotube Field-Effect Transistors, *Anal. Chem.* 79: 782–787.

Maehashi, K., Matsumoto, K., Kerman, K., Takamura, Y. & Tamiya, E. (2004). Ultrasensitive Detection of DNA Hybridization Using Carbon Nanotube Field-Effect Transistors, *Jpn. J. Appl. Phys.* 43: L1558–L1560.

Maehashi, K., Matsumoto, K., Takamura, Y. & Tamiya, E. (2009). Aptamer-Based Label-Free Immunosensors Using Carbon Nanotube Field-Effect Transistors, *Electroanalysis* 21: 1285–1290.

Maehashi, K., Ohno, Y., Inoue, K. & Matsumoto, K. (2004). Chirality selection of single-walled carbon nanotubes by laser resonance chirality selection method, *Appl. Phys. Lett.* 85: 858–860.

Martnez, M. T., Tseng, Y.-C., Ormategui, N., Loinaz, I., Eritja, R. & Bokor, J. (2009). Label-Free dna Biosensors Based on Functionalized Carbon Nanotube Field Effect Transistors, *Nano Lett.* 9: 530–536.

Meric, I., han, M. Y., Young, A. F., Ozyilmaz, B., Kim, P. & Shepard, K. L. (2008). Current saturation in zero-bandgap, topg-ated graphene field-effect transistors, *Nat. Nanotechnol.* 3: 654–659.

Minot, E. D., Janssens, A. M., Heller, I., Dekker, H. A. H. C. & Lemay, S. G. (2007). Carbon nanotube biosensors: The critical role of the reference electrode, *Appl. Phys. Lett.* 91: 093507.

Mohanty, N. & Berry, V. (2008). Graphene-Based Single-Bacterium Resolution Biodevice and Dna Transistor: Interfacing Graphene Derivatives with Nanoscale and Microscale Biocomponents, *Nano Lett.* 8: 4469–4476.

Nagashio, K., Nishimura, T., Kita, K. & Toriumi, A. (2008). Mobility Variations in Mono- and Multi-Layer Graphene Films, *Appl. Phys. Express* 2: 025003.

Novoselov, K. S., Geim, A. K., Morozov, S. V., Jiang, D., Zhang, Y., Dubonos, S. V., Grigorieva, I. V. & Firsov, A. A. (2004). Electric Field Effect in Atomically Thin Carbon Films, *Science* 306: 666–669.

Ohno, Y., Maehashi, K., Yamashiro, Y. & Matsumoto, K. (2009). Electrolyte-gated graphene field-effect transistors for detecting ph and protein adsorption, *Nano Lett.* 9: 3318–3322.

Palaniappan, A., Goh, W. H., Tey, J. N., Wijaya, I. P. M., Moochhala, S. M., Liedberg, B. & Mhaisalkar, S. G. (2010). Aligned carbon nanotubes on quartz substrate for liquid gated biosensing, *Biosens. Bioelectron.* 25: 1989–1993.

Pan, H., Feng, Y. P. & Lin, J. Y. (2004). Ab initio study of OH-functionalized single-wall carbon nanotubes, *Phys. Rev. B* 70: 245425.

Qazi, M., Vogt, T. & Koley, G. (2007). Trace gas detection using nanostructured graphite layers, *Appl. Phys. Lett.* 91: 233101.

Robinson, J. T., Perkins, F. K., Snow, E. S., Wei, Z. & Sheehan, P. E. (2008). Reduced Graphene Oxide Molecular Sensors, *Nano Lett.* 8: 3137–3140.

Rosenblatt, S., Yaish, Y., Park, J., Gore, J., Sazonova, V. & McEuen, P. L. (2002). High Performance Electrolyte Gated Carbon Nanotube Transistors, *Nano Lett.* 2: 869–872.

Saito, R., Dresselhaus, G. & Dresselhaus, M. S. (1998). *Physical Properties of Carbon Nanotubes*, Imperial College Press, London.

Schedin, F., Geim, A. K., Morozov, S. V., Hill, E. W., Blake, P., Katsnelson, M. I. & Novoselov, K. S. (2007). Detection of individual gas molecules adsorbed on graphene, *Nat. Mater.* 6: 652–655.

Shan, C., Yang, H., Song, J., Han, D., Ivaska, A. & Niu, L. (2009). Direct Electrochemistry of Glucose Oxidase and Biosensing for Glucose Based on Graphene, *Anal. Chem.* 81: 2378–2382.

Shang, N. G., Papakonstantinou, P., McMullan, M., Chu, M., Stamboulis, A., Potenza, A., Dhesi, S. S. & Marchetto, H. (2008). Catalyst-Free Efficient Growth, Orientation and Biosensing Properties of Multilayer Graphene Nanoflake Films with Sharp Edge Planes, *Adv. Funct. Mater.* 18: 3506–3514.

Star, A., Gabriel, J.-C. P., Bradley, K. & Grüner, G. (2003). Electronic Detection of Specific Protein Binding Using Nanotube fet Devices, *Nano Lett.* 3: 459–463.

Wu, H., Wang, J., Kang, X., Wang, C., Wang, D., Liu, J., Aksay, I. A. & Lin, Y. (2009). Glucose biosensor based on immobilization of glucose oxidase in platinum nanoparticles/graphene/chitosan nanocomposite film, *Talanta* 80: 403–406.

Yamamoto, Y., Ohno, Y., Maehashi, K. & Matsumoto, K. (2009). Noise Reduction of Carbon Nanotube Field-Effect Transistor Biosensors by Alternating Current Measurement, *Jpn. J. Appl. Phys.* 48: 06FJ01.

Yamamoto, Y., Ohno, Y., Maehashi, K. & Matsumoto, K. (2010). Electrical Detection of Negatively Charged Proteins Using n-Type Carbon Nanotube Field-Effect Transistor Biosensors, *Jpn. J. Appl. Phys.* 49: 02BD10.

Yang, W., Ratinac, K. R., Ringer, S. P., Thordarson, P., Gooding, J. J. & Braet, F. (2010). Carbon Nanomaterials in Biosensors: Should You Use Nanotubes or Graphene?, *Angew. Chem., Int. Ed.* 49: 2114–2138.

Zheng, G., Patolsky, F., Cui, Y., Wang, W. U. & Lieber, C. M. (2005). Multiplexed electrical detection of cancer markers with nanowire sensor arrays, *Nat. Biotechnol.* 23: 1294–1301.

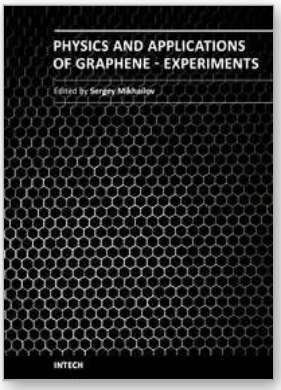

Physics and Applications of Graphene - Experiments

Edited by Dr. Sergey Mikhailov

ISBN 978-953-307-217-3
Hard cover, 540 pages
Publisher InTech
Published online 19, April, 2011
Published in print edition April, 2011

The Stone Age, the Bronze Age, the Iron Age... Every global epoch in the history of the mankind is characterized by materials used in it. In 2004 a new era in material science was opened: the era of graphene or, more generally, of two-dimensional materials. Graphene is the strongest and the most stretchable known material, it has the record thermal conductivity and the very high mobility of charge carriers. It demonstrates many interesting fundamental physical effects and promises a lot of applications, among which are conductive ink, terahertz transistors, ultrafast photodetectors and bendable touch screens. In 2010 Andre Geim and Konstantin Novoselov were awarded the Nobel Prize in Physics "for groundbreaking experiments regarding the two-dimensional material graphene". The two volumes Physics and Applications of Graphene - Experiments and Physics and Applications of Graphene - Theory contain a collection of research articles reporting on different aspects of experimental and theoretical studies of this new material.

InTech Europe
University Campus STeP Ri
Slavka Krautzeka 83/A
51000 Rijeka, Croatia
Phone: +385 (51) 770 447
Fax: +385 (51) 686 166
www.intechopen.com

InTech China
Unit 405, Office Block, Hotel Equatorial Shanghai
No.65, Yan An Road (West), Shanghai, 200040, China
中国上海市延安西路65号上海国际贵都大饭店办公楼405单元
Phone: +86-21-62489820
Fax: +86-21-62489821